Nuclear Activity of MLA Immune Receptors Links Isolate-Specific and Basal Disease-Resistance Responses

Qian-Hua Shen, *et al.*

Science **315**, 1098 (2007);
DOI: 10.1126/science.1136372

Nuclear Activity of MLA Immune Receptors Links Isolate-Specific and Basal Disease-Resistance Responses

Qian-Hua Shen,[1] Yusuke Saijo,[1] Stefan Mauch,[1] Christoph Biskup,[2] Stéphane Bieri,[3] Beat Keller,[3] Hikaru Seki,[1]* Bekir Ülker,[1]† Imre E. Somssich,[1] Paul Schulze-Lefert[1]‡

Plant immune responses are triggered by pattern recognition receptors that detect conserved pathogen-associated molecular patterns (PAMPs) or by resistance (R) proteins recognizing isolate-specific pathogen effectors. We show that in barley, intracellular mildew A (MLA) R proteins function in the nucleus to confer resistance against the powdery mildew fungus. Recognition of the fungal avirulence A10 effector by MLA10 induces nuclear associations between receptor and WRKY transcription factors. The identified WRKY proteins act as repressors of PAMP-triggered basal defense. MLA appears to interfere with the WRKY repressor function, thereby de-repressing PAMP-triggered basal defense. Our findings reveal a mechanism by which these polymorphic immune receptors integrate distinct pathogen signals.

Plants have evolved two classes of immune receptors, each of which recognizes non-self molecular structures. One class involves membrane-resident pattern recognition receptors (PRRs) that detect pathogen-associated molecular patterns (PAMPs) such as bacterial flagellin or chitin, a component of fungal cell walls (*1*). During interactions with virulent parasites, PRRs confer weak immune responses that attenuate pathogen growth and contribute to basal defense (*1*). Reduced PAMP-mediated defense probably results from successful host defense suppression by pathogen effectors (*1*). Resistance (R) proteins represent a second, mainly intracellular, immune receptor class having the capacity to directly or indirectly detect isolate-specific pathogen effectors, encoded by avirulence (*AVR*) genes (*1*). PRR-triggered immune responses are tightly linked to mitogen-activated protein kinase signaling, the accumulation of reactive oxygen species (ROS), and the activation of defense-related genes involving WRKY transcription factors (TFs) (*2*). Immediate signaling components of effector-activated R proteins are unknown. However, R protein–triggered immune responses are also linked to ROS accumulation and defense-gene activation but differ quantitatively and kinetically from basal defense, often leading to host cell suicide at invasion sites (*3*). This points to a convergence of PRR- and R protein–triggered signaling, but the nodes and mechanisms enabling plants to integrate signals from these two receptor classes remain elusive.

The polymorphic barley *mildew A* (*MLA*) *R* locus encodes allelic receptors containing an N-terminal coiled-coil (CC) structure, a central nucleotide-binding (NB) site, and a leucine-rich repeat (LRR) region. MLA receptors share >90% sequence identity but recognize isolate-specific *Blumeria graminis* f sp. *hordei* effectors (*4*–*7*). *MLA1*/*MLA6* hybrid analyses revealed that recognition specificity is determined by different but overlapping LRRs and a C-terminal non-LRR region (CT) (*6*). MLA steady-state levels are critical for effective resistance and are subject to control by cytosolic heat-shock protein 90 (Hsp90) and the co-chaperone–like proteins RAR1 and SGT1 (*8*, *9*). Recently, the *B. graminis* effector AVR_{A10}, which is recognized by MLA10, was isolated and shown to belong to a diversified gene family comprising more than 30 paralogs (*5*, *10*). The availability of the cognate *MLA10* and AVR_{A10} gene pair, as well as the cell-autonomous nature of MLA resistance to *B. graminis* upon transient gene expression in single epidermal cells, enabled us to elucidate effector-dependent receptor functions (*5*, *7*, *10*).

Nuclear activity of MLA receptors. Biochemical fractionation of leaf protein extracts from transgenic barley lines expressing epitope-tagged *MLA1* or *MLA6* detected the majority of the receptor in the soluble fraction (*8*). To examine the subcellular distribution of MLA, we biolistically delivered a DNA plasmid encoding MLA10 tagged with yellow fluorescent protein (YFP) into leaf epidermal cells and recorded YFP fluorescence by confocal imaging (Fig. 1A, upper panel). MLA10-YFP localized to the cytoplasm and the nucleus. Biolistic delivery of wild-type *MLA10* or *MLA10-YFP* constructs into single epidermal cells comparably restricted *B. graminis* growth in an AVR_{A10}-dependent manner (Fig. 1B), demonstrating activity of the MLA10-YFP fusion protein. To determine the functional role of the nuclear MLA10 pool, we fused a nuclear export signal (NES) to the C terminus of MLA10-YFP (*11*). Expression of the MLA10-YFP-NES construct revealed undetectable nuclear fluorescence signals in the majority (>80%) of epidermal cells despite clearly visible cytoplasmic YFP fluorescence. In the remaining cells, nuclei were indirectly marked by a YFP halo (Fig. 1A, middle panel). If this difference in the subcellular distribution between MLA10-YFP-NES– and MLA10-YFP–expressing cells were due to a functional NES, then amino acid substitutions predicted to render the NES nonfunctional (nes) (*11*) should restore nuclear accumulation of a corresponding MLA10-YFP-nes fusion protein. Indeed, the subcellular YFP fluorescence distribution patterns of cells expressing MLA10-YFP-nes or MLA10-YFP were indistinguishable (Fig. 1A, bottom panel). Inoculation with *B. graminis* expressing AVR_{A10} showed that the MLA10-YFP-NES receptor variant was inactive, whereas MLA10-YFP-nes restored activity to MLA10 wild-type–like levels (Fig. 1B). Together these data strongly imply that the nuclear pool of MLA10 is essential for its disease-resistance function. This is unexpected because MLA lacks known nuclear localization signals.

We next analyzed stable transgenic barley lines containing a single copy of functional epitope-tagged *MLA1* driven by native 5′ regulatory sequences (*8*). We purified nuclei from leaves of 7-day-old seedlings before and after inoculation with *B. graminis* isolates expressing or lacking the cognate AVR_{A1} effector. Immunoblot analyses detected MLA1-HA in both nuclear extracts and nuclei-depleted soluble fractions (Fig. 1C). A time-course experiment revealed an apparent increase of the nuclear MLA1-HA pool in the incompatible interaction (12, 18, and 24 hours after spore inoculation) as compared to the compatible interaction (Fig. 1C; similar results were obtained with protein extracts from leaf epidermal tissue). This demonstrates the existence of a nuclear pool for a second MLA receptor, is indicative of dynamic changes of the nuclear pool during the immune response, and suggests that the intracellular distribution of MLA10-YFP observed in the single-cell system probably reflects its physiological locations.

***Hv*WRKY1/2 TFs interact with the MLA CC domain.** We constructed yeast two-hybrid baits encoding single or multiple domains of MLA1 or MLA6 CC-NB-LRR-CT receptors and screened a barley prey cDNA library derived from healthy and *B. graminis*–challenged leaf epidermal tissue (Fig. 2A) (*8*, *12*). The bait MLA

[1]Department of Plant Microbe Interactions, Max-Planck-Institut für Züchtungsforschung, Carl-von-Linné-Weg 10, D-50829 Köln, Germany. [2]Institute of Physiology II, Friedrich-Schiller-University of Jena, Teichgraben 8, D-07740 Jena, Germany. [3]Institute of Plant Biology, University of Zürich, Zollikerstrasse 107, 8008 Zürich, Switzerland.

*Present address: RIKEN Plant Science Center, 1-7-22 Suehirocho, Tsurumi-ku, Yokohama, Kanagawa, 230-0045, Japan.

†Present address: School of Biological and Biomedical Sciences, Durham University, Science Site, South Road, Durham DH1 3LE, UK.

‡To whom correspondence should be addressed. E-mail: schlef@mpiz-koeln.mpg.de

CC_{1-46} (an invariant sequence in all known MLA receptors) identified four interactors. Two were dismissed because of their predicted localization in chloroplasts and mitochondria. One identified prey cDNA encoded an N-terminally truncated version of a WRKY domain–containing TF, designated *Hv*WRKY2 (*Hv*, *Hordeum vulgare*) (Fig. 2A; GenBank accession number AJ853838). A highly sequence-related homolog, designated *Hv*WRKY1 (GenBank accession number AJ536667), sharing 72% sequence similarity and identical domains and motifs (fig. S2), was subsequently isolated and also found to interact with the MLA CC_{1-46} bait by targeted yeast two-hybrid experiments. To characterize MLA and *Hv*WRKY1/2 TFs interactions, we performed directed yeast two-hybrid assays using truncated and full-length receptor and TF variants. Although interactions were found with truncated forms of the receptor and the TFs (Fig. 2A), the full-length MLA6 bait failed to interact with all tested *Hv*WRKY1 or *Hv*WRKY2 prey variants despite the presence of comparable amounts of the LexA-MLA fusion proteins (fig. S1). This might indicate requirements for intra- and intermolecular interactions in vivo.

To examine whether MLA directly interacts with *Hv*WRKY1/2, we performed in vitro pull-down assays. A hemagglutinin (HA) epitope–tagged MLA1 CC_{1-166} fragment was expressed in a wheat germ in vitro translation system and subsequently incubated with glutathione *S*-transferase (GST)–*Hv*$WRKY2_{107-319}$ or GST alone purified from *Escherichia coli* lysates. Immunoblot analysis of GST pull-down precipitates with HA antibodies revealed the presence of MLA1 CC_{1-166} in GST-*Hv*$WRKY2_{107-319}$ but not GST precipitates (Fig. 2B). This is consistent with a physical interaction between the MLA1 CC and the *Hv*WRKY2 TF.

***HvWRKY1/2* repressor functions.** To elucidate the functional role of *HvWRKY1* and *HvWRKY2* in immune responses to *B. graminis*, we first examined their contribution to basal defense mechanisms by virus-induced gene silencing (VIGS) during a compatible interaction. Barley seedlings were inoculated with a barley stripe mosaic virus (BSMV) vector harboring antisense fragments of *HvWRKY1* (BSMV-WRKY1as) or *HvWRKY2* (BSMV-WRKY2as) or control vectors (Fig. 3A) (*13*). Two weeks after BSMV infection, leaves were inoculated with a virulent *B. graminis* isolate, and the frequency of fungal microcolonies on the leaf surface was microscopically scored 48 hours later. Whereas leaves inoculated with the control vectors supported a frequency of 15 ± 2% and 19 ± 2% microcolonies, respectively, significantly reduced levels were found with BSMV-WRKY1as and BSMV-WRKY2as [7 ± 2% and 9 ± 3% (Fig. 3A); the fourth leaf was used for VIGS experiments that show a higher level of basal defense than did the first true leaf used for single-cell gene expression studies]. This is consistent with and extends previous data showing heightened resistance to a different virulent *B. graminis* iso-

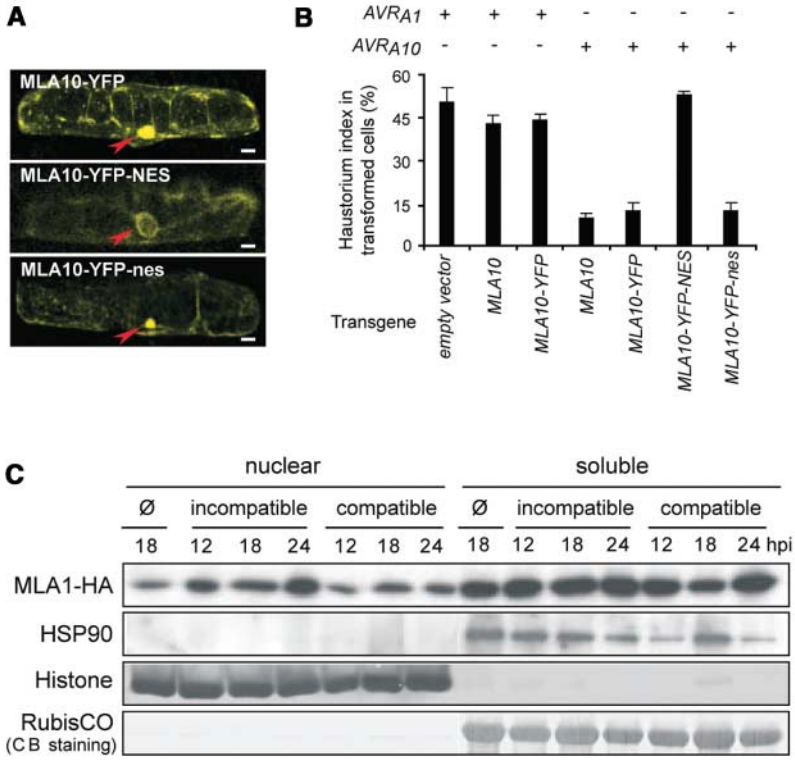

Fig. 1. The nuclear MLA10 fraction mediates race-specific resistance. (**A**) Confocal image of a barley leaf epidermal cell expressing MLA10-YFP [upper panel, three-dimensional (3D) reconstruction], MLA10-YFP-NES (middle, 2D *z* plane), and MLA10-YFP-nes (lower panel, 2D *z* plane). Cytoplasmic strands traversing the vacuole are also visible. Arrowheads mark the nuclei, Scale bar, 10 μm. (**B**) Haustorium index in leaf epidermal cells upon biolistic codelivery of the indicated plasmid vectors and *GUS* reporter. Bombarded leaves were inoculated with *B. graminis* isolates expressing AVR_{A1} or AVR_{A10}. Fungal haustoria were microscopically scored 48 hours after inoculation. Data were obtained from three independent experiments. (**C**) Western blot of MLA1-HA in nuclear and soluble fractions of healthy or *B. graminis*–challenged leaves. Purified nuclear and nuclei-depleted soluble fractions were prepared from leaves of a transgenic line expressing MLA1-HA (*8*) at the indicated time points [hours post inoculation (hpi)] after inoculation with *B. graminis* isolates expressing or lacking AVR_{A1} (incompatible or compatible). All fractions were subjected to immunoblot analyses. This loading represents an approximately 16-fold overrepresentation of nuclear proteins on a per-tissue amount basis. Ø, non-inoculated controls. Histone H3, cytosolic Hsp90, and Coomassie blue (CB) staining of ribulose-1,5-bisphosphate carboxylase-oxygenase (RubisCO) were used as fraction markers.

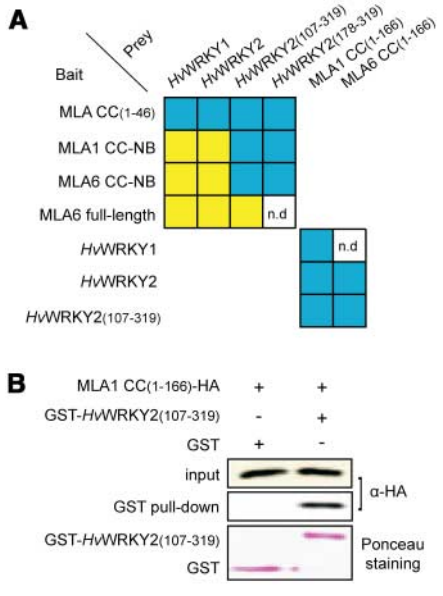

Fig. 2. *Hv*WRKY1/2 TFs interact with the MLA CC domain. (**A**) Results of yeast two-hybrid assays between bait fusions of the LexA DNA binding domain and prey fusions of the B42 activation domain containing either MLA1/6 or *Hv*WRKY1/2 sequences as indicated. Blue, detected interactions; yellow, undetectable interactions; n.d., not determined. (**B**) Immunoblot analysis of GST and GST-*Hv*$WRKY2_{107-319}$ pull-down precipitates. GST or GST-*Hv*$WRKY2_{107-319}$ were incubated with HA epitope–tagged MLA1 CC_{1-166} before GST pull-downs. Ten μl of the mixtures was subjected to immunoblot analysis with antiserum to HA as an input control. MLA1 CC_{1-166} was detected by antiserum to HA, GST-$WRKY2_{107-319}$, and GST by Ponceau staining.

late upon *HvWRKY1* single-cell silencing in the leaf epidermis (*14*), suggesting that *Hv*WRKY1 and *Hv*WRKY2 act as repressors of basal defense to virulent *B. graminis*.

We tested this hypothesis through *HvWRKY2* overexpression experiments during compatible interactions. Biolistic delivery of a *HvWRKY2* construct, driven by the strong ubiquitin promoter, into single leaf epidermal cells resulted in supersusceptibility in different genetic backgrounds harboring *MLA1-HA*, *MLA6-HA*, or wild-type *MLA10* (Fig. 3B; similar results were obtained with *HvWRKY1*). Overexpression of *SUSIBA2*, a barley WRKY TF functioning in sugar signaling (*15*), did not alter the *B. graminis* infection type (Fig. 3B), indicating that sequence motifs other than the shared WRKY DNA binding domain (*16*) contribute to the *HvWRKY1/2*-dependent supersusceptible phenotype. The contrasting infection phenotypes observed upon overexpression or gene silencing of *HvWRKY1/2* are consistent with their presumed roles as repressors of basal defense. *HvWRKY1* and *HvWRKY2* expression was strongly (≥20 fold), rapidly (within 3 hours), and transiently activated upon *B. graminis* challenge in both compatible and *MLA*-specified incompatible interactions (fig. S3A) approximately 10 hours before differential infection phenotypes became microscopically visible. This, and the observation that a similarly strong and even faster *HvWRKY1* and *HvWRKY2* activation occurred upon treatment of leaves with the bacterial flg22 PAMP (fig. S3B), support our hypothesis that both genes are components of PAMP-triggered basal defense.

Next we investigated the importance of the physical association between the invariant MLA CC domain and *Hv*WRKY1/2 during incompatible interactions. We reasoned that if MLA receptors function through interference with *Hv*WRKY1/2 repressor activity in basal defense, then single-cell overexpression of *HvWRKY1/2* might block MLA function because of inappropriate timing and/or TF levels. Indeed, single-cell *HvWRKY2* overexpression fully compromised tested *MLA1-HA*–, *MLA10*-, and *MLA12*-specified immune responses to *B. graminis* isolates expressing cognate Avr_A effectors (Fig. 3C; similar results were obtained with *HvWRKY1*). We previously showed that *MLA12* single-cell overexpression alters the resistance kinetics, but not specificity, so that the growth of a larger proportion of fungal germlings is terminated earlier in comparison to *MLA12* wild-type plants (*6*). To test whether overexpression of the receptor can negate the effect of overexpressed *HvWRKY2*, we co-delivered *HvWRKY2* with *MLA10* or *MLA12*. This still compromised both MLA-specified immune responses (Fig. 3C), indicating that in wild-type plants *HvWRKY2* expression must be tightly controlled to ensure proper MLA function. *SUSIBA2* WRKY overexpression did not interfere with tested *MLA1-HA*–triggered immunity, again illustrating that only particular WRKY TFs can interfere with immune responses to *B. graminis* (Fig. 3C). *HvWRKY2* overexpression also failed to compromise *MLG*-triggered race-specific as well as *mlo*-mediated race-nonspecific resistance to *B. graminis* (Fig. 3C) (*17*, *18*). This is consistent with previous results demonstrating separate genetic pathways for race-specific and *mlo*-mediated resistance (*19*) and revealing the existence of at least one *HvWRKY2* independent *R* gene–triggered immune response to *B. graminis*.

Effector-dependent association between MLA and *Hv*WRKY2. To directly test associations between the MLA receptor and *Hv*WRKY2 in plants, we labeled the proteins with the yellow (YFP)– or blue [cyan fluorescent protein (CFP)]–shifted variants of the green fluorescent protein (GFP), respectively. Upon biolistic delivery of the corresponding DNA plasmids into epidermal cells, functional MLA10-YFP and functional CFP-*Hv*WRKY2 fusion proteins colocalized in epidermal nuclei (fig. S4, A and B; CFP-*Hv*WRKY2 exclusively localizes to the nucleus in all experiments described below). To test protein associations in the presence or absence of the cognate AVR_{A10} pathogen effector (*10*), we monitored for Förster resonance energy transfer (FRET) between the fluorescence tags of MLA10-YFP and CFP-*Hv*WRKY2. In this study, we adopted a quantitative noninvasive fluorescence lifetime imaging (FLIM) approach to detect FRET (fig. S5). To calculate FRET efficiency (E) the lifetime of the donor in the presence of the acceptor (τ_{DA}) only needs to be compared with its lifetime in the absence of the acceptor (τ_D): $E = 1 - \tau_{DA}/\tau_D$. This approach has the advantage that FRET and control measurements can be performed in different cells because fluorescence lifetimes are independent of the actual fluorophore concentration.

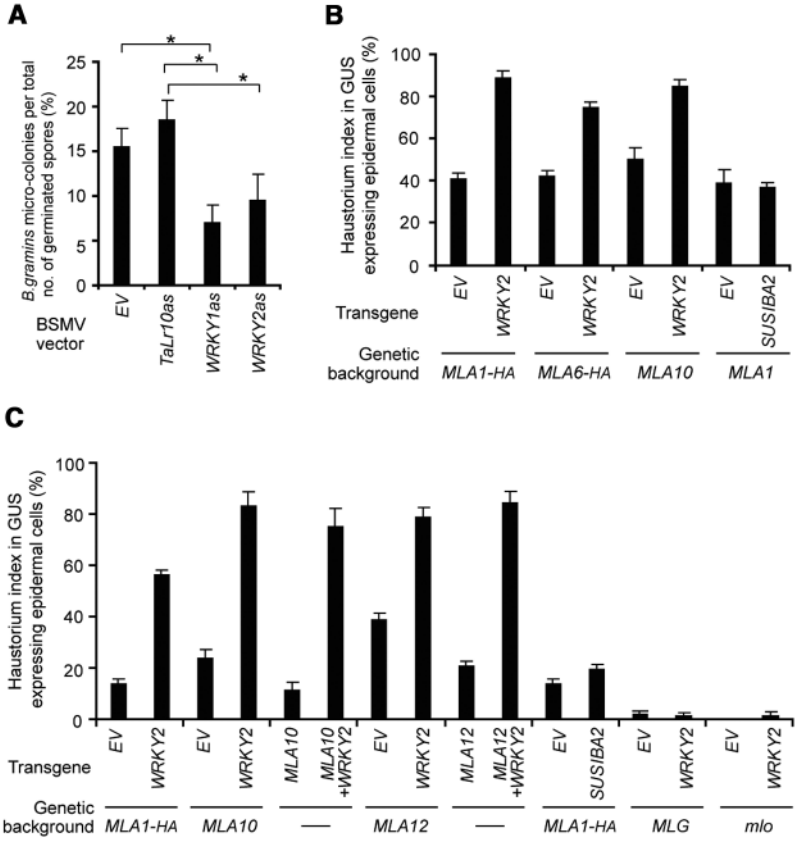

Fig. 3. *Hv*WRKY1/2 TFs repress basal and interfere with *MLA*-triggered immune responses. (**A**) *B. graminis* microcolony formation on barley leaves after BSMV-mediated *HvWRKY1* or *HvWRKY2* silencing. BSMV empty vector (BSMV-EV) and BSMV-TaLr10as were used as controls. BSMV-TaLr10as harbors an antisense fragment of the 3′ untranslated region of wheat *TaLr10* that is of similar length to BSMV-WRKY1as or BSMV-WRKY2as. Mean values of microcolony formation are based on the microscopic analysis of at least 600 interaction sites at 48 hours after inoculation with *B. graminis* conidiospores of virulent isolate A6. Asterisk indicates significant difference at $P < 0.05$. (**B**) Haustorium index in leaf epidermal cells after inoculation with *B. graminis* conidiospores of virulent isolates A6 or K1. Empty DNA vectors (EV) or plasmids expressing *HvWRKY2* or *HvSUSIBA2* were biolistically codelivered with the *GUS* reporter into epidermal cells of the indicated genetic backgrounds. (**C**) Haustorium index in leaf epidermal cells after inoculation with *B. graminis* conidiospores of avirulent isolates A6 or K1. EVs or plasmids expressing the indicated transgenes were biolistically codelivered with the *GUS* reporter into epidermal cells of the indicated genetic backgrounds.

We measured the lifetimes of free CFP and CFP fusion proteins as a control. The average lifetime of free CFP was 2.53 ± 0.02 ns (mean ± SEM, n = 8 nuclei) (fig. S6F). Unexpectedly, the average CFP lifetime in nuclei expressing the CFP-*Hv*WRKY2 fusion was reduced to 2.12 ± 0.02 ns (n = 24; Fig. 4A and fig. S6F), indicating possible homo-FRET between the CFP tags of associated CFP-*Hv*WRKY2 fusion proteins (*20*). In contrast, the average CFP lifetime of CFP-SUSIBA2 (2.47 ± 0.01 ns, n = 5; fig. S6, C and F) was close to that of unfused CFP (2.53 ± 0.02). To directly test for *Hv*WRKY2 dimerization, we generated a YFP-*Hv*WRKY2 construct and co-delivered it with CFP-*Hv*WRKY2 into epidermal cells. A dramatic reduction of the average CFP lifetime to 1.29 ± 0.04 ns (n = 7) was recorded in nuclei coexpressing the fusion proteins (fig. S6, A and F). To rule out the possibility that CFP lifetime reduction was due to unspecific associations between the fluorescent tags, we coexpressed as a control CFP-*Hv*WRKY2 and unfused YFP. Nuclei coexpressing these two proteins showed an average CFP lifetime of 2.03 ± 0.01 ns (n = 12; fig. S6, B and F), which is close to the average CFP lifetime of CFP-WRKY2 alone (2.12 ± 0.02 ns). Collectively, this provides strong in vivo evidence for homomeric *Hv*WRKY2 associations.

In the coexpression experiments, a measured lifetime was considered to be significantly (P < 0.003) shorter when it was more than 3 SD lower than the respective control values. For CFP-WRKY2, the threshold was calculated to be 1.92 ns. Thus, upon coexpression with potential interactors, lifetimes <1.92 ns can be attributed to FRET. For CFP-SUSIBA2, the calculated threshold was 2.39 ns. We measured the CFP lifetime upon coexpression of functional CFP-*Hv*WRKY2 and MLA10-YFP (2.00 ± 0.03 ns, n = 12; Fig. 4B and fig. S6F) and found that it did not differ significantly (P < 0.01) from the average CFP lifetime of nuclei coexpressing CFP-*Hv*WRKY2 and free YFP (2.03 ± 0.01 ns). Thus, there is no evidence for constitutive associations between the immune receptor and the TF, which is consistent with undetectable interactions between full-length MLA and *Hv*WRKY1/2 in the yeast two-hybrid experiments (Fig. 2). However, cells subjected to cotransformation of CFP-*Hv*WRKY2, MLA10-YFP, and the *B. graminis* AVR_{A10} effector, which is recognized by MLA10, produced a broad CFP lifetime distribution not seen in any other tested combinations, ranging from 1.32 to 2.17 ns (Fig. 4C and fig. S6F). Ten out of 27 (37%) CFP lifetime measurements yielded lifetimes that were significantly shorter than that of the CFP-*Hv*WRKY2 control (Fig. 4A), indicating AVR_{A10}-stimulated associations between MLA10 and *Hv*WRKY2. That a portion of the measured CFP lifetimes does not differ from the control measurements could indicate that the stoichiometry between the three proteins and putative auxiliary factors is critical and/or that the association between receptor and WRKY TF is only transient by nature.

When we coexpressed CFP-*Hv*WRKY2, MLA10-YFP, and the *B. graminis* effector AVR_{K1} [an AVR_{A10} homolog recognized by the MLK R protein (*10*)], the average CFP lifetime (2.06 ± 0.03 ns, n = 14) did not differ significantly from the lifetime found in nuclei coexpressing CFP-*Hv*WRKY2 and MLA10-YFP (Fig. 4D and fig. S6F). Furthermore, replacement of CFP-*Hv*WRKY2 by CFP-SUSIBA2 in combinations with MLA10-YFP and AVR_{A10} or AVR_{K1} failed to generate a pronounced broadening of the CFP lifetime distribution [lifetimes were 2.42 ± 0.03 ns (n = 11) and 2.43 ± 0.02 ns (n = 11), respectively; fig. S6, D to F]. Together, this corroborates the ability of MLA immune receptors to interact with particular WRKY family members in the nucleus and supports the notion of an AVR_{A10}-dependent physical association between MLA10 and *Hv*WRKY2.

The FLIM-FRET data were substantiated by using the conventional acceptor photobleaching method (APB-FRET). To estimate the extent of FRET, the donor fluorescence intensity is measured before and after the acceptor chromophore is bleached. Donor fluorescence intensity increases in those cases where FRET has occurred before bleaching. Such an increase in CFP intensity was observed only in nuclei coexpressing CFP-*Hv*WRKY2, MLA10-YFP, and AVR_{A10} (fig. S7) but not in nuclei coexpressing CFP-*Hv*WRKY2 and YFP, or CFP-*Hv*WRKY2, MLA10-YFP, and AVR_{K1} (fig. S7). This independently confirms the AVR_{A10}-dependent physical association between MLA10 and *Hv*WRKY2 in nuclei.

***AtWRKY18/40* repressor functions.** WRKY TFs belong to large gene families in *Arabidopsis* and in rice (*21*, *22*). *Arabidopsis AtWRKY18*, *AtWRKY40*, and *AtWRKY60* (*At*, *Arabidopsis thaliana*) and rice *OsWRKY28* and *OsWRKY71* (*Os*, *Oryza sativa*) show the highest sequence relatedness to *HvWRKY1* and *HvWRKY2* (fig. S2). The deduced proteins form a distinct subgroup of group II WRKYs containing a leucine zipper (LZ) domain thought to be involved in homo- and/or heterocomplex formation (*23*, *24*). *AtWRKY18*, *AtWRKY40*, and *AtWRKY60* have been recently implicated in repressing basal defense to virulent hemibiotrophic *Pseudomonas syringae* (*24*). We tested mutant lines of these *Arabidopsis WRKY* family members by inoculation with the virulent powdery mildew

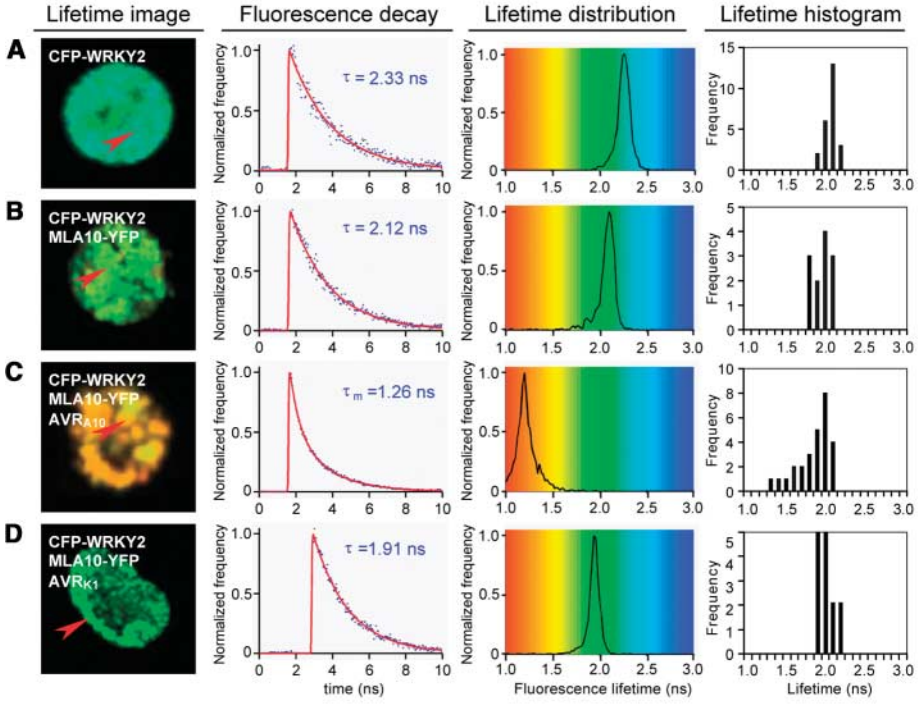

Fig. 4. (**A** to **D**) *Hv*WRKY2 and MLA10 association is AVR_{A10}-dependent. FLIM measurements in barley epidermal nuclei expressing the indicated protein(s) are shown. (Left column) CFP fluorescence lifetime image of the nucleus of a representative cell expressing the indicated protein(s). The average fluorescence lifetime obtained for each pixel is encoded by color as indicated by the scale in the middle right column. (Middle left column) CFP fluorescence decay curve measured for the pixel marked by the red arrowhead in the left column. The decay curve was approximated by a mono- or biexponential function as described in the supporting online material. (Middle right column) CFP fluorescence lifetime distribution throughout the nucleus shown in the lifetime image. (Right column) Histogram of mean CFP fluorescence lifetimes obtained for all measured nuclei expressing the indicated protein(s). Bar heights represent the number of nuclei whose mean lifetime falls within the indicated 0.1-ns range.

Golovinomyces orontii (*24*) (and our collections). Although single *Atwrky18*, *Atwrky40*, or *Atwrky60* mutant plants and *Atwrky18/60* or *Atwrky40/60* double mutants retained Col-0 wild-type–like susceptibility, the *Atwrky18/40* and *Atwrky18/40/60* triple mutant lines were almost fully resistant (Fig. 5, A and B). This reveals redundant *At*WRKY18 and *At*WRKY40 activities and points to a conserved repressor function of the dicot and monocot homologs in basal defense.

Although *Atwrky18/40* double mutants do not constitutively express defense-associated genes (*24*), genome-wide gene expression profiling experiments upon inoculation with virulent *P. syringae* DC3000 revealed that a subset of 23 genes accumulates earlier and is 3.5-fold or more up-regulated in the *Atwrky18/40* double mutant but not in *Atwrky18* or *Atwrky40* single mutants (table S1). This subset contains 21 PAMP-responsive genes, including the 6-fold up-regulated *SID2*, which encodes isochorismate synthase 1, required for salicylic acid biosynthesis, and is a major contributor to basal defense against *G. orontii* (*25*, *26*). Thus, mutants lacking the *At*WRKY18/40 repressors retain the ability to execute stimulus-dependent defense-gene expression and the response appears to be exaggerated. These findings imply the existence of an *At*WRKY18/40-dependent feedback repression system as an intrinsic control feature of basal defense.

Conclusions. Few host factors have been identified that directly interact with intracellular NB-LRR proteins and participate in receptor function. A subset of these, including cytosolic Hsp90, determines R protein steady-state levels, possibly by regulated folding of monomeric R proteins and/or preactivated R protein–containing complexes (*27*). *Arabidopsis* RIN4 interacts with the NB-LRR type R proteins RPM1 and RPS2, forming a preactivation receptor complex at the plasma membrane that permits indirect recognition of the cognate *P. syringae* effectors AvrRpm1 and AvrRpt2, respectively (*28*, *29*). Whether AVR_{A10} is directly or indirectly recognized by the cytoplasmic and/or nuclear MLA10 pool remains unknown. However, unrestricted growth of AVR_{A10}-expressing *B. graminis* after coexpression of *MLA10* and *HvWRKY2* (Fig. 3C) is difficult to reconcile with a scenario in which the TF serves as the effector target that indirectly activates the receptor. We could not detect association of the functional, fluorochrome-tagged MLA10 and *Hv*WRKY2 by FRET-FLIM in the absence of AVR_{A10}. This suggests that the specific, AVR_{A10}-stimulated nuclear association between receptor and TF is a postrecognition event involving activated MLA. Altered intramolecular interactions in the NB-LRR R proteins Rx and Bs2 probably accompany their effector-dependent activation (*30*, *31*). Because MLA recognition specificity is determined by the sequence-divergent LRR-CT region (*6*), direct or indirect effector-induced modulations of the MLA LRR-CT may similarly lead to intramolecular interaction changes, in turn permitting an association of the invariant CC domain with *Hv*WRKY1/2.

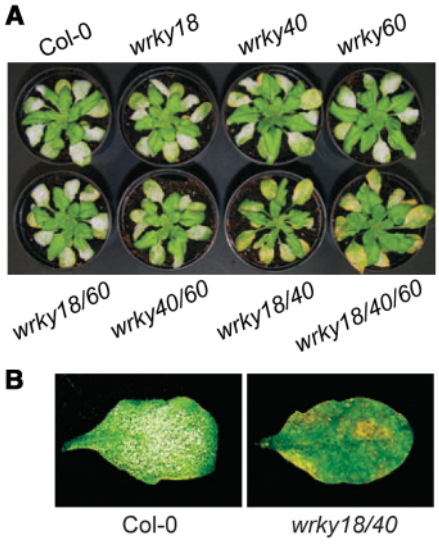

Fig. 5. *Atwrky18/40* double mutant plants are resistant to *G. orontii*. (**A**) Infection phenotypes of *Arabidopsis* plants 10 days after inoculation with virulent *G. orontii*. Plant genotypes are indicated. (**B**) Macroscopic leaf infection phenotype of a representative Col-0 and *Atwrky18/40* plant shown in (A).

Our data suggest that the transcriptional machinery of PAMP-triggered basal defense is a direct target of MLA, thereby providing a link between PRR- and R protein–triggered immunity. Although transcriptional reprogramming of the host during incompatible versus compatible interactions differs only quantitatively and kinetically (*3*), it is difficult to determine whether the typically weaker and/or less sustained defense-related gene expression during compatible interactions is the consequence of effector-mediated defense suppression or is an intrinsic feature of PAMP-triggered basal defense. The retained pathogen-dependent but exaggerated activation of a subset of defense-related genes in *Arabidopsis Atwrky18 wrky40* double mutants is consistent with the existence of at least one negative feedback system operating in PAMP-mediated basal defense. Because enhanced defense against virulent *G. orontii* in *Atwrky18/40* plants was accompanied by extensive leaf cell death (Fig. 5), *At*WRKY18/40-dependent repression might restrict the output of PAMP-triggered basal defense below a detrimental threshold and, at the same time, function as a hair trigger of the primed immune system for R protein–dependent defense potentiation driving host cells into suicide. Given that *AtWRKY18/40* are functionally homologous to *HvWRKY1/2*, it is reasonable to hypothesize that the observed genetic interference (Fig. 3C) and physical association (Figs. 2 and 4) between MLA and *Hv*WRKY1/2 during incompatible interactions with *B. graminis* result in derepression of PAMP-triggered basal defense (fig. S8). This regulatory logic of MLA function could explain why, after biolistic delivery of AVR_{A10} into host epidermal cells of *MLA10* genotypes (that is, in the absence of PAMPs), most cells remain alive (*10*). Direct targeting of PAMP-activated *Hv*WRKY1/2 repressors by MLA receptors also implies a short signaling pathway that may not require genuine *R* gene–specific signaling components.

Plant and animal innate immune systems are thought to have evolved independently from each other (*32*). Accordingly, biochemical constraints might have contributed to the engagement of structurally related components for immune functions in both phyla, including the CATERPILLER superfamily, which encompasses plant NB-LRR R and mammalian NOD proteins (*33*, *34*). CATERPILLER proteins have either demonstrated or anticipated roles as microbial component sensors to control immune and inflammatory responses. In this context, direct targeting of *Hv*WRKY1/2 repressors by MLA R proteins in the nucleus is reminiscent of the nuclear CATERPILLER CIITA function, which acts through direct association with DNA binding proteins to regulate the expression of all major histocompatibility complex class II and other genes important in antigen presentation (*34*). Domain fusion events between a WRKY and NB-LRR domain in two *Arabidopsis* proteins, including the RRS1-R R protein–to–*Ralstonia solanacearum* infection (*35*), suggest similar transcription machinery–associated functions of plant immune receptors.

References and Notes

1. J. D. G. Jones, J. L. Dangl, *Nature* **444**, 323 (2006).
2. T. Asai *et al.*, *Nature* **415**, 977 (2002).
3. Y. Tao *et al.*, *Plant Cell* **15**, 317 (2003).
4. D. Halterman, F. Zhou, F. Wei, R. P. Wise, P. Schulze-Lefert, *Plant J.* **25**, 335 (2001).
5. D. A. Halterman, R. P. Wise, *Plant J.* **38**, 215 (2004).
6. Q. H. Shen *et al.*, *Plant Cell* **15**, 732 (2003).
7. F. Zhou *et al.*, *Plant Cell* **13**, 337 (2001).
8. S. Bieri *et al.*, *Plant Cell* **16**, 3480 (2004).
9. I. Hein *et al.*, *Plant Physiol.* **138**, 2155 (2005).
10. C. J. Ridout *et al.*, *Plant Cell* **18**, 2402 (2006).
11. W. Wen, J. L. Meinkoth, R. Y. Tsien, S. S. Taylor, *Cell* **82**, 463 (1995).
12. Materials and methods are available as supporting material on *Science* Online.
13. S. Holzberg, P. Brosio, C. Gross, G. P. Pogue, *Plant J.* **30**, 315 (2002).
14. C. Eckey *et al.*, *Plant Mol. Biol.* **55**, 1 (2004).
15. C. X. Sun *et al.*, *Plant Cell* **15**, 2076 (2003).
16. K. Yamasaki *et al.*, *Plant Cell* **17**, 944 (2005).
17. R. Büschges *et al.*, *Cell* **88**, 695 (1997).
18. R. Görg, K. Hollricher, P. Schulze-Lefert, *Plant J.* **3**, 857 (1993).
19. C. Peterhänsel, A. Freialdenhoven, J. Kurth, R. Kolsch, P. Schulze-Lefert, *Plant Cell* **9**, 1397 (1997).
20. I. Gautier *et al.*, *Biophys. J.* **80**, 3000 (2001).
21. B. Ulker, I. E. Somssich, *Curr. Opin. Plant Biol.* **7**, 491 (2004).
22. Z. Xie *et al.*, *Plant Physiol.* **137**, 176 (2005).
23. R. S. Cormack *et al.*, *Biochim. Biophys. Acta Gene Struct. Express.* **1576**, 92 (2002).
24. X. P. Xu, C. H. Chen, B. F. Fan, Z. X. Chen, *Plant Cell* **18**, 1310 (2006).

25. J. Dewdney *et al.*, *Plant J.* **24**, 205 (2000).
26. M. C. Wildermuth, J. Dewdney, G. Wu, F. M. Ausubel, *Nature* **414**, 562 (2001).
27. P. Schulze-Lefert, *Curr. Biol.* **14**, R22 (2004).
28. M. J. Axtell, B. Staskawicz, *Cell* **112**, 369 (2003).
29. D. Mackey, B. F. Holt III, A. Wiig, J. L. Dangl, *Cell* **108**, 743 (2002).
30. R. T. Leister *et al.*, *Plant Cell* **17**, 1268 (2005).
31. G. J. Rairdan, P. Moffett, *Plant Cell* **18**, 2082 (2006).
32. F. M. Ausubel, *Nat. Immunol.* **6**, 973 (2005).
33. W. Strober, P. J. Murray, A. Kitani, T. Watanabe, *Nat. Rev. Immunol.* **6**, 9 (2006).
34. J. P. Y. Ting, D. L. Kastner, H. M. Hoffman, *Nat. Rev. Immunol.* **6**, 183 (2006).
35. L. Deslandes *et al.*, *Proc. Natl. Acad. Sci. U.S.A.* **100**, 8024 (2003).
36. We thank C. Ridout and C. Jansson for providing various plasmids; Z. Chen (Purdue University) for providing *Arabidopsis wrky* single and triple mutants; and E. Schmelzer, E. Logemann, A. Reinstaedler, M. Hallstein, and H. Häweker for technical support. This work was supported by funds from the Max Planck Society, a Deutsche Forschungsgemeinschaft grant (SFB670) to Q.-H. S., and a European Union–BIOEXPLOIT grant to Y.S.

Supporting Online Material
www.sciencemag.org/cgi/content/full/1136372/DC1
Materials and Methods
Figs. S1 to S8
Table S1
References

16 October 2006; accepted 14 December 2006
Published online 21 December 2006;
10.1126/science.1136372
Include this information when citing this paper.

The Triple-Ring Nebula Around SN 1987A: Fingerprint of a Binary Merger

Thomas Morris[1,2] and Philipp Podsiadlowski[1]*

Supernova 1987A, the first naked-eye supernova observed since Kepler's supernova in 1604, defies a number of theoretical expectations. Its anomalies have long been attributed to a merger between two massive stars that occurred some 20,000 years before the explosion, but so far there has been no conclusive proof that this merger took place. Here, we present three-dimensional hydrodynamical simulations of the mass ejection associated with such a merger and the subsequent evolution of the ejecta, and we show that this accurately reproduces the properties of the triple-ring nebula surrounding the supernova.

Supernova 1987A in the Large Magellanic Cloud was one of the major astronomical events of the 1980s, but it was highly unusual. The progenitor star, Sk −69°202, was one of the surprises. Massive stars similar to the progenitor of SN 1987A are expected to end their evolution as red supergiants, but Sk −69°202 was a blue supergiant. Moreover, the outer layers of the star were highly enriched in helium (*1*), suggesting that some nuclear processed material from the core had been mixed into the envelope by a nonstandard mixing process (*2*). Most notably, the supernova was surrounded by a complex triple-ring nebula (*3*, *4*) consisting of material that was ejected from the progenitor some 20,000 years before the explosion in an almost axi-symmetric but very nonspherical manner. Together, this evidence indicates that a dramatic event affected the progenitor some 20,000 years before the explosion, most likely the merger of two massive stars (*5*).

A merger was first suggested to explain some of the asymmetries of the supernova ejecta (*6*). Later it was realized that a binary merger would also explain the blue progenitor and its main chemical anomalies (*7*–*9*). This hypothesis has since been confirmed by detailed stellar, hydrodynamical simulations of the slow merger of two massive stars (*10*). However, the origin of the triple-ring nebula has so far not found a satisfactory explanation.

The triple-ring nebula consists of three overlapping rings in projection. The supernova occurred at the center of the inner ring, and the outer rings are in planes almost parallel to the central ring plane but displaced by 0.4 pc above and below the central ring plane. Notably, these outer rings do not form the limb-brightened projection of an hourglass nebula, as in some of the early models for the nebula (*11*–*13*), but form instead dense, ringlike density enhancements (*4*). Previous attempts to model the nebula have involved interacting winds in a binary (*14*, *15*), a photoionization-driven instability (*16*), mass ejection during a binary merger (*17*), or magnetically controlled ejection (*18*), but none of these has been able to fully explain both the detailed geometry and the kinematical properties of the nebula.

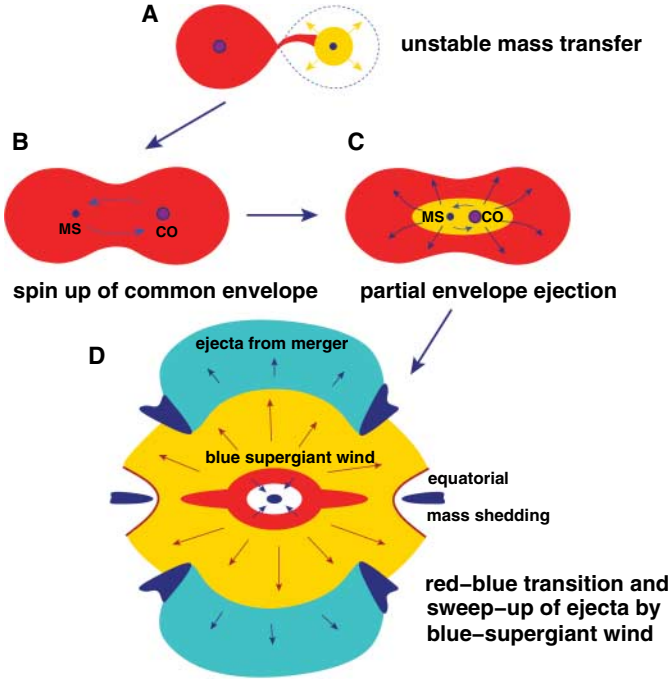

Fig. 1. Schematic diagram showing the formation of the triple-ring nebula. The system initially consisted of a binary with two stars of ~15 and ~5 $M_{\odot}$ with an orbital period longer than ~10 years. Mass transfer is dynamically unstable, leading to the merger of the two components in (**A**) a common envelope and (**B**) the spin-up of the envelope. MS, main-sequence companion; CO, carbon-oxygen core. (**C**) The release of orbital energy due to the spiral in of the companion leads to the partial ejection of the envelope. (**D**) After the merging has been completed, the merged object evolves to become a blue supergiant, shedding its excess angular momentum in an equatorial outflow. In the final blue-supergiant phase, the energetic wind from the blue supergiant sweeps up all of the previous structures, producing the triple-ring nebula.

[1]Department of Astrophysics, University of Oxford, Oxford OX1 3RH, UK. [2]Max-Planck Institut für Astrophysik, Garching 85741, Germany.

*To whom correspondence should be addressed. E-mail: podsi@astro.ox.ac.uk